THE PENNSYLVANIA STATE UNIVERSITY
SCHREYER HONORS COLLEGE

DEPARTMENT OF AEROSPACE ENGINEERING

Numerical Verification of Asymptotic Dynamic Soaring Control Strategy

Zhenda Li
Spring 2019

A thesis
submitted in partial fulfillment
of the requirements
for baccalaureate degree
in Aerospace Engineering
with honors in Aerospace Engineering

Reviewed and approved by the following:

Jack W. Langelaan
Associate Professor of Aerospace Engineering
Thesis Supervisor

Cengiz Camci
Professor of Aerospace Engineering
Honors Advisor

Amy Pritchett
Professor of Aerospace Engineering
Department Head of Aerospace Engineering

Abstract

This thesis discusses and verifies a control strategy to achieve autonomous dynamic soaring for small fixed wing aircraft in numerical simulation. Dynamic soaring is a bio-inspired flight technique that allows an aerial vehicle to fly without engine power. With proper flight maneuver, the vehicle is able to convert wind energy to kinetic energy. A numerical simulation for a small fixed-wing aircraft soaring in a shear wind-field is built first. An autonomous control policy is found by numerical optimization over control inputs at each time step in the numerical wind shear environment. The performance of this control strategy is then assessed based on its sustainability and the total energy harvested.

Table of Contents

List of Figures

List of Tables

Acknowledgements

I would like to thank my advisor, Jack Langelaan, for his advice in this thesis. I would like to thank everyone I met in the Department of Aerospace Engineering at Penn State. I would also thank Penn State library. Finally, I would like to thank my family for their endless support.

Chapter 1

Introduction to Dynamic Soaring

1.1 Dynamic Soaring and Motivation

Dynamic soaring is a flying technique by which an aerial vehicle maintains energy-neutral flight without any power input by repetitively crossing the wind shear[1]. Dynamic soaring is considered a strategy to achieve engine-less long-endurance high-speed flight for autonomous fixed wing aircraft [2]. By harvesting energy from wind, a small unmanned aerial vehicle (UAV) similar to the small glider shown in 1.1 can better perform missions such as wildlife monitoring, weather surveillance [3], and search and rescue operations [4]. Taking one step further from the energy-neutral flight, dynamics soaring shows its potential in energy extraction and power regeneration for UAV [4]. To the author's knowledge, dynamic soaring has not yet been demonstrated by an autonomous aircraft. However, with continuing advances in small aircraft, embedded computation, and lightweight sensor systems, autonomous dynamic soaring will be possible in the near future.

Dynamic soaring is bio-inspired. It was first described in 1883 by Lord Rayleigh, who observed that some birds can stay aloft without flapping their wings and proposed a mechanism by which they maintain flight [5] [3]. In fact, albatrosses—a sea bird shown in Figure 1.2—can travel thousands of kilometers with minimum muscle work [6]. There are flight recordings [7] indicating distances of 15,200 km travelled in a single foraging trip. They can also maintain a high flight speed by taking advantage of favorable winds. The ground speeds can be greater than 127 km/h for more than 8 hours [8]. The flight records of the albatross are impressive and it is therefore tempting to apply the same flight strategy to a UAV.

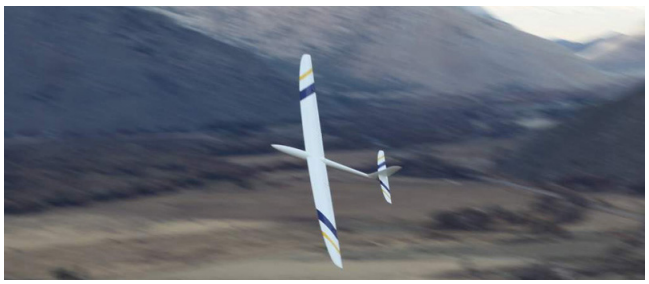

Figure 1.1: Radio-controlled Dynamic Glider at Weldon, California

Figure 1.2: Albatross Soaring above the Sea

Dynamic soaring exploits spatial gradients in a steady wind field. Typically, vertical gradients (more specifically, gradients where the wind speed increases with altitude) are used in dynamic soaring. These gradients occur near flat terrain (or over open ocean), at the leeward side of ridges, and (to a lesser extent) when there is a sudden change in wind speed across a temperature inversion. Deittert et al.[9] state the boundary layer shear of sufficient strength to permit dynamic soaring by albatrosses occurs over 90% of the time over the southern oceans.

1.2 Types of Dynamic Soaring

The first type of dynamic soaring forms a closed loop trajectory, which is referred to the circular dynamic soaring trajectory in this thesis. An example is shown in Figure 1.3. With a circular trajectory, the aerial vehicle can stay in altitude by repetitively crossing the wind shear. For every circular dynamic soaring cycle, the aerial vehicle starts at the low point of the trajectory with its heading direction perpendicular to the horizontal wind. It then turn into the wind and climbs through the wind shear at the same time. As the vehicle reaches the high point of the trajectory, it turns away from the wind and dives back to the start point. Circular dynamic soaring is valuable in energy generation mission. With the wind field remains **largely** unchanged for every flight cycle, the aerial vehicle can obtain better estimation of the wind field and possibly find a better control policy to extract more energy. This dynamic soaring mode is typical of that flown by radio-controlled glider pilots.

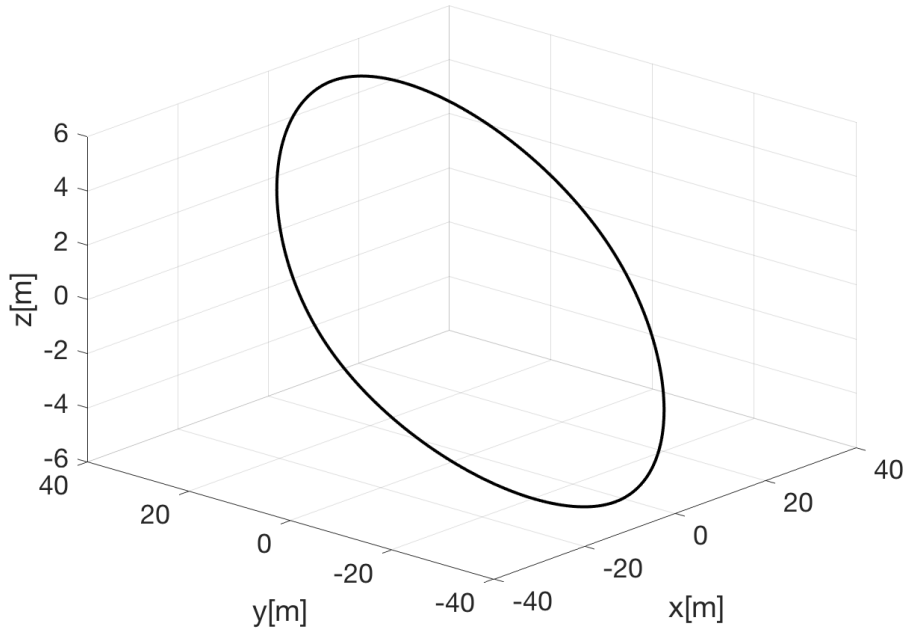

Figure 1.3: Circular Trajectory

While the first type of dynamic soaring is ubiquitous in the literature, the second type is the main concern of this thesis. It is a periodic trajectory that allows the aerial vehicle to fly forward in the direction perpendicular to the horizontal wind and extract energy simultaneously. An example is shown in 1.4. It is termed as the asymptotic dynamic soaring trajectory [10]. The required maneuver for asymptotic dynamic soaring is similar to circular dynamic soaring in the beginning. The vehicle starts at the same location and flies into the wind and climb. As it reaches the high point of the trajectory, it turns away from the wind and dive. It then instead banks away from the initial point and fly forward to the next low point. It is the strategy albatrosses are observed to use to travel in a long range. Unlike circular dynamic soaring, asymptotic dynamic soaring is more valuable in travel. However, it is also more difficult, because as the aerial vehicle progresses, the wind field is likely to be different than that in its start location. The goal of this thesis is to verify an optimization process that can find solution to asymptotic dynamic soaring.

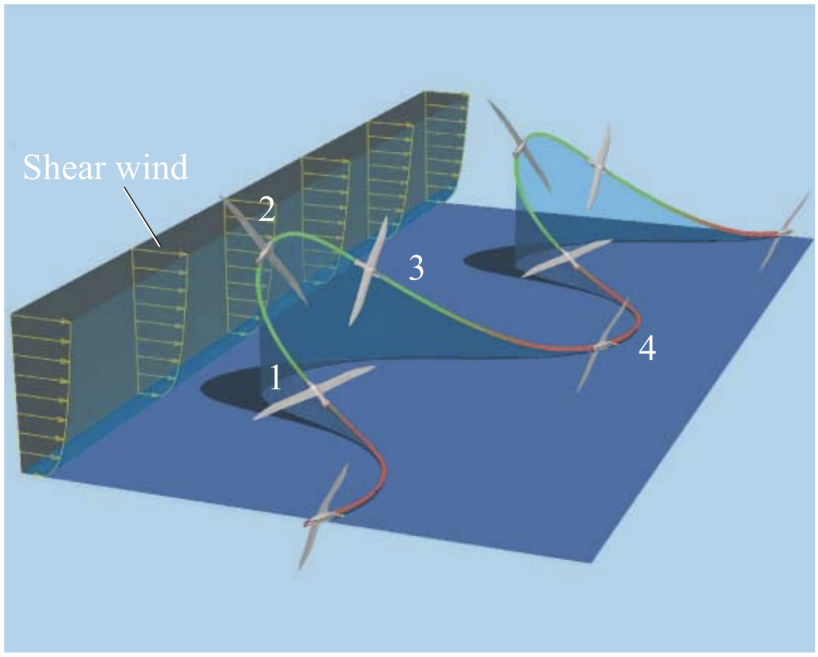

Figure 1.4: Asymptotic Trajectory

Note that other dynamic soaring trajectories exist (for example, a figure 8-trajectory, as in Figure 1.5). However, they are out of the scope of this thesis.

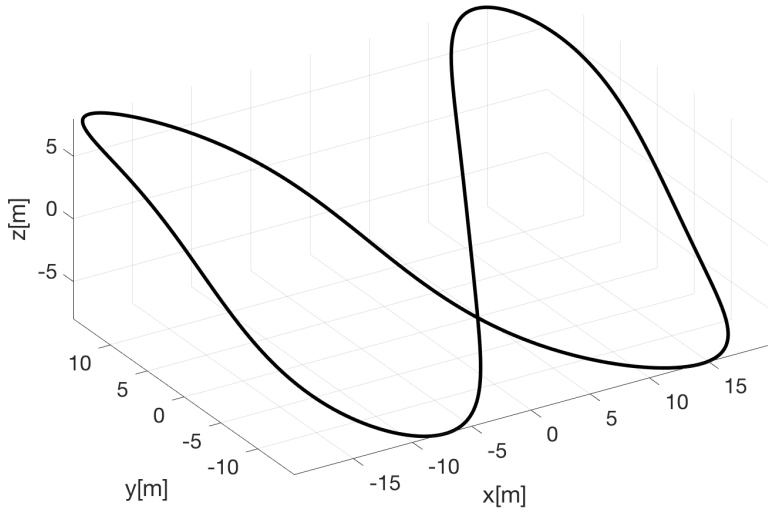

Figure 1.5: Figure 8 Shape Trajectory

1.3 Related work

The study in dynamic soaring has started a century ago and is still ongoing. Back in 1883, Lord Rayleigh [5] correctly developed a model to show how birds can convert energy from the wind field and proposed a dynamics soaring strategy called the Rayleigh's cycle, which justifies dynamic soaring mathematically in the first time. Later, researches [10][6][4] take advantages of the numerical method. A dynamic soaring solution can be achieved numerically with the full knowledge of a steady wind profile. Recently, dynamics soaring research is actively filling more details in dynamic soaring. Bird [3] estimates the map of wind field with which the dynamics soaring is planned. Sachs [6] discusses the maximum travel speed by dynamic soaring and its relation to the wind speed. Long [4] shows the possibility power regeneration over flat terrains by dynamic soaring, an indirect way to achieve a long endurance mission. Garvilovic [11] investigates stochastic wind field and found that the wind with higher turbulence intensity potentially provides more energy for transfer. There are also a few novel approaches to solve dynamic soaring. Montella[12] use deep Q learning in reinforcement learning to approach the dynamic soaring problem. More energy can be extracted from the environment by learning algorithm.

1.4 Summary of Contributions

The main focus of this work is the development and verification of a method to compute dynamic soaring trajectories in a fixed wind shear environment. In addition, this work:

- outlines the equations of motion of an aircraft flying in a spatially-varying wind field
- outlines two mathematical models of wind shear
- proposes control inputs that can be easily implemented on currently-available autopilot hardware
- implements a trajectory optimization algorithm that enables energy-neutral flight
- demonstrates the utility of the proposed approach in simulation.

1.5 Reader's Guide

- Chapter 2 formulates the equations of motion of the soaring dynamics, with their assumptions listed and discussed. It also provides a wind field function to model the wind shear applicable to dynamic soaring. An algorithm for numerical simulation is also setup.
- Chapter 3 set up the optimization by defining the optimization variables, cost functions, and constraint. It then shows and discusses the simulated results with the solution found by the optimizer.
- Chapter 4 concludes this thesis and illustrates future study in dynamics soaring.

Chapter 2

Problem Statement and System Models

In this chapter, a mathematical model is first introduced in section 2.1 in order to study dynamic soaring rigorously. Assumption and simplification are discussed and justified. Equations of motion will be shown and examined. Wind field is then modeled in a separated section 2.2. Several wind shear models will be discussed with a focus on the sigmoid function based wind shear model, which is eventually applied in the numerical simulation. With the mathematical model developed in first two sections, section 2.3 will transform the model from continuous space to discrete space, in which numerical simulation can be performed. The last section will formally state the dynamic soaring problem in term of the model and simulation developed in this chapter.

2.1 Aircraft Model

The aircraft model used in this work is described in Hendricks [13] and later used either directly or with minor changes by many recent researches in dynamic soaring [2] [4] [6] [10] [14]. The main assumption made is the point mass assumption, which simplifies the dynamics for study and implementation. It also allows further generalize the result[4]. It is assumed that all the forces and moment act on the center of mass of the aircraft. Thus, equations of motion with 3 degrees of freedom is expected. The second important assumption is that the wind blows in a fixed direction—in this thesis, parallel to the inertial y-axis. It is considered a reasonable assumption for dynamic soaring in a quasi-steady shear flows [14]. Then, the wind velocity vector can be expressed as $\mathbf{w} = -w(z)\hat{\mathrm{y}}$, where w is the magnitude of the wind as a function of the altitude z. A detailed discussion about the selection of this wind field function can be found in the next section. Thirdly, since it is a glider intending to achieve dynamic soaring, thrust is set to be zero.

There are total three forces acting on the aircraft. They are the aerodynamic lift $\mathbf{L}$, drag $\mathbf{D}$, and gravity mg. The equation of motions in the inertial frame of reference can be written as

$$m(\dot{\mathbf{v}} - \dot{\mathbf{w}}) = -mg\hat{\mathbf{z}} + \mathbf{L} + \mathbf{D} \tag{2.1}$$

where $\mathbf{v}$ is the air velocity vector. It is convenient to create a non-inertial "wind-fixed" reference frame[14], which is composed by the first axis coincident with the air velocity vector, the second axis in the inertial vertical plane and orthogonal with the first axis, the third orthogonal with both the first and second axis, as shown in Figure 2.1

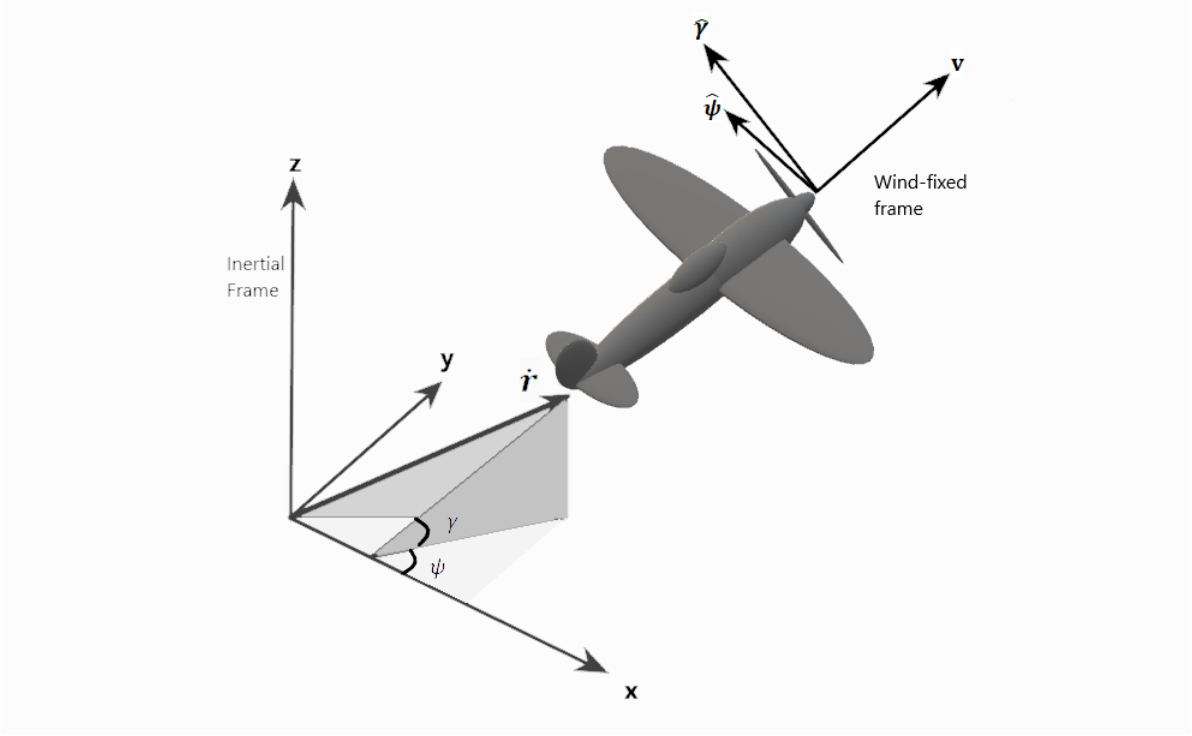

Figure 2.1: Wind-fixed Reference Frame

Writing the equation of motions (equation 2.1) in the "wind-fixed" reference frame by kinematics,

$$\begin{aligned} m\dot{v} &= -D - mg\sin\gamma + m\dot{w}\cos\gamma\sin\psi \\ mV\dot{\gamma} &= L\cos\phi - mg\cos\gamma - m\dot{w}\sin\gamma\sin\psi \\ mV\dot{\psi}\cos\gamma &= L\sin\phi + m\dot{w}\cos\psi \end{aligned} \tag{2.2}$$

where the L, D, and v are the magnitude of lift, drag, and air velocity respectively. ϕ, γ, and ψ are the bank angle, flight path angle, and heading angle. Notice that equation 2.2 is a nonlinear system of ordinary differential equations with respect to time, with three states of v, γ, and ψ. Also note that, the system is not complete by itself—it contains variables other than its three states. Those "missing pieces" are $\dot{w}$, L, D, and ϕ.

$\dot{w}$ is the time derivative of the wind speed experienced by the aircraft. By the chain rule, it can be expressed in terms of $\dot{z}$, which can also be obtained by kinematics.

$$\dot{z} = V \sin\gamma \tag{2.3}$$

$$\dot{w} = \frac{dw}{dz}\dot{z} = \frac{dw}{dz} V \sin\gamma \tag{2.4}$$

Although the other two spatial states x and y in an inertial frame are not required to solve the system 2.2, they are calculated for future evaluation and better understanding of the simulation. By kinematics,

$$\dot{x} = v\cos\gamma\cos\psi \tag{2.5}$$

$$\dot{y} = -w + v\cos\gamma\sin\psi \tag{2.6}$$

Lift L and drag D are the two forces required to solve the nonlinear system 2.2. They are modeled by an empirical method. Lift is modeled by the product of the dynamic pressure $1/2\rho v^2$, wing area S, and the lift coefficient. That is

$$L = \frac{1}{2}\rho v^2 S C_L$$

where the lift coefficient C_L is calculated by a linear model as

$$C_L = C_{L_\alpha}(\theta - \gamma) + C_{L_o} \tag{2.7}$$

where the difference between the pitch angle θ and flight path angle γ is angle of attack. In another word, the lift coefficient is proportional to the angle of attack in a slope of C_{L_α} with empirical intercept C_{L_o}. C_{L_α} can be obtained by experiments or approximated with the wing aspect ratio AR and an efficiency term τ_e obtained from the lifting line theory.

$$C_{L_\alpha} = \frac{2\pi}{1 + \frac{2\pi}{\pi\tau_e AR}}$$

The aerodynamics drag D is modeled similar to the lift. D is the product of the dynamic pressure, wing area, and the drag coefficient C_D,

$$C_D = (C_{d_o} + \frac{C_L^2}{\pi AR e_o})$$

which is composed of a constant profile drag coefficient C_{d_o} found empirically and a term that incorporates the components of drag that are dependent of lift coefficient. e_o is the Oswald's efficiency.

The last two missing variables in the nonlinear system 2.2 are the pitch angle θ and the bank angle ϕ. They are the control inputs. In the numerical simulation, the dynamic soaring control law produces $\phi(t)$ and $\theta(t)$ and feed them into the equations of motion 2.2. For potential flight in

reality, pitch angle θ can be controlled by the elevator on the glider and the bank angle ϕ can be controlled by the ailerons. Note that standard autopilot modules such as the Pixhawk allow direct control over bank angle and pitch angle, which makes this formulation amenable to hardware implementation. Now, the dynamics model for the aircraft is complete.

2.2 Wind Shear Model

In this section, the wind field function $w(z)$ is defined. As shown in section 2.1, $\dot{w}(z)$ plays an important role in the nonlinear system. It is also the key for to success of dynamic soaring—energy harvesting from wind field. The wind field in reality is stochastic, which makes the study of dynamic soaring difficult. The steady wind profile is assumed to simplify the problem. There are several types of wind field used by different researchers in dynamic soaring. The first type of the wind field function is following,

$$w_{nd} = \frac{w_o}{1 + e^{-\frac{z}{\delta}}} \tag{2.8}$$

where w_{nd} is dimensionless wind field profile. Notice that w_{nd} is a sigmoid function scaling by the wind intensity factor w_o. This wind field will be referred as the sigmoid wind field in this thesis. δ is the wind shear term. A large δ results in a weaker wind shear—smaller velocity gradient with respect to z. The wind field intensity w_o and the shear strength δ are the two features that determine the wind field. To obtain the dimensional wind field function $w(z)$, the w is scaling by a characteristic speed V_c. V_c is the speed flown at a lift coefficient of 1. Note that its magnitude is determined by the glider's wing loading.

$$W = w_{nd} V_C = w(\frac{2mg}{\rho S})^{\frac{1}{2}} \tag{2.9}$$

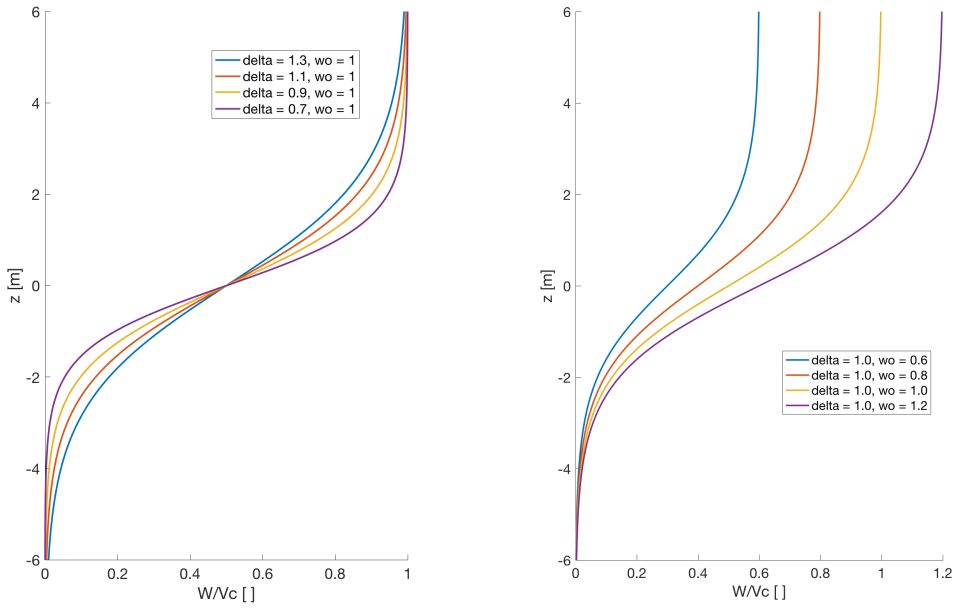

(a) fixed $w_o = 1$ with different δ

(b) fixed $\delta = 1$ with different w_o

Figure 2.2: Sigmoid Wind Field

To demonstrate the sigmoid wind field function, Figure 2.2 shows the wind profile with different shear factor δ and intensity factor w_o chosen. As expected, with a smaller wind shear strength factor δ, the wind speed profile changes more rapidly with the altitude. With a larger wind intensity factor w_o, the magnitude of the wind speed profile becomes larger. Note that the mean speed of the wind field is located at the datum $z = 0$, which is above the ground. The wind shear is largest also at the datum $z = 0$. With the altitude z deviates from the datum, the wind shear drops asymptotically to zero. The region in wind field with significant wind shear is usually referred as the shear layer, whose center is located at $z = 0$ for the sigmoid wind field. In this sigmoid wind field, the shear layer is where most of the energy is extracted from the wind field. The sigmoid wind field can approximate the wind field behind the ridge as shown in Figure 2.3 [2]. The sigmoid wind field is implemented in this thesis and some other dynamics soaring researches as well [10] [2].

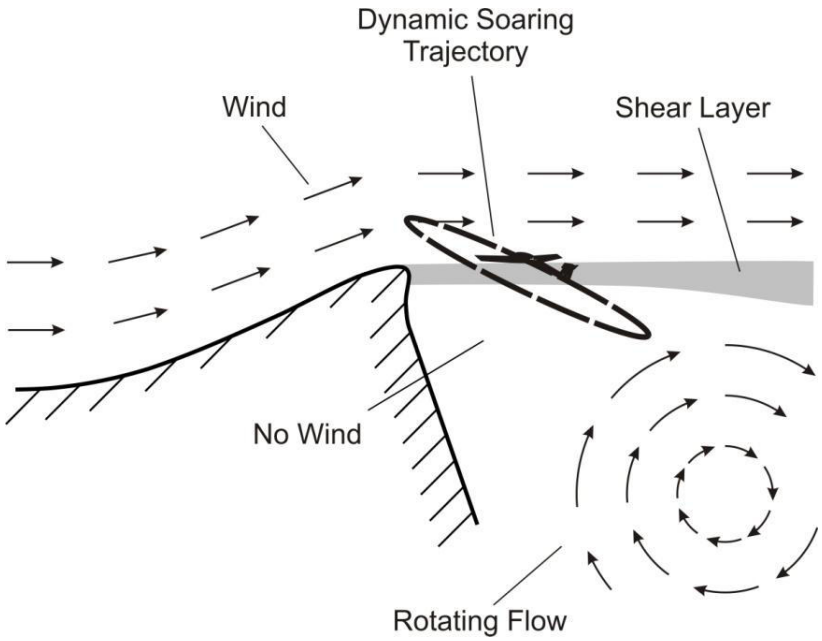

Figure 2.3: Ridge Dynamic Soaring[2]

Two sigmoid wind field in dimensional speed is shown in Figure 2.4.They will be applied in the simulation later in this thesis.

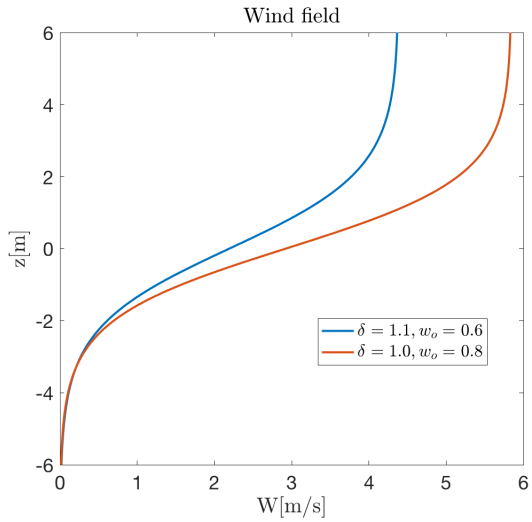

Figure 2.4: Dimensional Wind Field Examples

The other major wind field model for dynamic soaring is a logarithmic model [6] [15]. Wind speed profile is modeled as a logarithmic function scaling by a constant. An example wind speed profile is shown in Figure 2.5. Note that the maximum wind speed gradient is at altitude $h = 0$ and the wind speed grows unbounded. The shape of the wind profile is similar to the boundary

layer over a flat plate in the classic of fluid mechanics. The logarithmic model well approximates the wind field of dynamic soaring in flat terrains and above the sea, shown earlier in Figure 1.4.

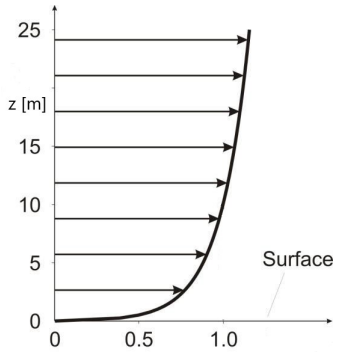

Figure 2.5: Logarithmic Wind Profile[6]

2.3 Numerical Simulation

The dynamics model in section 2.1 is a non-linear system of ODEs. An analytical solution can be found in certain steady-state (i.e. constant speed) cases, but an analytic solution for dynamic soaring has not yet been found. A numerical method is applied in this thesis to practically tackle the dynamic soaring problem. With both the model in dynamics and wind field developed, it is not difficult to find a numerical solution of the system. Although there are many sophisticated methods to solve ODE system, the most straight-forward method—forward Euler method—is applied for efficient computation. The entire dynamic algorithm is shown in $\mathbf{Algorithm 1}$.

Algorithm 1: Dynamics Simulation

Result: States $\mathbf{x}$ in each time step
initialize $\mathbf{x_0}$;
for $t_0, t_1, t_2, .., t_i, .., t_{final}$ **do**
  $\phi_i, \theta_i = \mathbf{controller}(\mathbf{x_i})$;
  $W_i = \mathbf{windfield}(z_i)$;
  calculate $\dot{\mathbf{x}}_\mathbf{i}$ by equation of motion $2.2, 2.3, 2.5, 2.6$;
  $\mathbf{x_{i+1}} = \mathbf{x_i} + \Delta t \times \dot{\mathbf{x}}_\mathbf{i}$;
  if *meet stop conditions* **then**
    $\mathbf{break}$;
  end
end

The algorithm takes the initial states $\mathbf{x_0}$ as input, which is the initial state vector $< x_0, y_0, z_0, V_0, \gamma_0, \psi_0 >$ and yields states for all the following time steps $\{\mathbf{x_i} | i = 1, 2, 3, ..., final\}$. For each time step i, the algorithm first obtains the control input—bank angle ϕ_i and pitch angle θ_i from the controller. In the numerical simulation, the wind speed in i^{th} step is found by the wind profile model shown in equation 2.8 and 2.9. Then, the state derivative terms $\dot{\mathbf{x}}_\mathbf{i}$ is calculated by the equations of motion

$2.2, 2.3, 2.5, 2.6$. The state $\mathbf{x_{i+1}}$ in the following time step is found by forward Euler integration. With the for-loop iterating through all time steps, states in every time step can be found. Stop conditions for the simulation can be formulated to early stop of the algorithm, for example, a lower bound for the altitude can be set for ground clearance. Without otherwise notification, the model parameter selected for the simulation in this thesis is chosen as shown in Table 2.1. The aircraft parameters are chosen based on the size of the potential UAV glider in application to dynamic soaring.

Model Parameter	**Values in Simulation**
m	$1.0kg$
S	$0.3m^2$
C_{d_o}	0.0125
e_o	0.53
AR	12
τ_e	0.8
C_{L_o}	0.2
Δt	$0.02sec.$

Table 2.1: Model Parameters

2.4 Problem Statement and Summary

In this chapter, the mathematical model for the soaring dynamics and wind field is formulated. A numerical simulation is also set up. The problem addressed in this thesis can be stated formally. Recall the ultimate goal is to achieve long-endurance flight for small fixed-wing glider by implementing dynamic soaring flight strategy. To achieve the goal, an intelligent system should be developed to control the vehicle to exploit the energy harvested from the wind field. The more energy the vehicle gained from the wind shear, a longer flight mission can be achieved. It thus becomes an optimization problem of a nonlinear ODE system over the control policy $\phi(t)$ and $\theta(t)$. A goal that is compatible with the mathematical model can be rigorously formulated into a cost function. A few candidate cost functions can be easily formulated. One of them is the total time the vehicle stays in altitude. It is a direct measures of the quality of the control policy and it fits the need in realistic application well. The cost function can be also formulated indirectly by introducing the total energy of the vehicle. Instead of measuring the total time a vehicle can stay on mission given a initial condition, the energy cost function examine the intelligent system's control policy indirectly by the total energy, which is a function of states and therefore applicable to every time step during the simulation. The energy cost function is eventually chosen in this thesis. Details about the choice of cost functions with their limitations and advantages can be found in section 3.2. The next chapter proposes a solution for this optimization problem.

Chapter 3

Trajectory Optimization

3.1 Design of the Solution

As demonstrated in Chapter 2, the dynamics system has two control inputs, namely, the bank angle $\phi(t)$ and the pitch angle $\theta(t)$ as functions of time. The final goal is to find appropriate functions $\phi(t)$ and $\theta(t)$ that can achieve dynamic soaring. There are a few criteria that these functions have to meet that is helpful to reduce the solution space for searching. First, both $\phi(t)$ and $\theta(t)$ are bounded. Depends on the aircraft, bank angle $\phi(t)$ and pitch angle $\theta(t)$ can range from -45° to 45° and from -20° and 20°. Second, since the pitch and bank angles are physically impossible to change rapidly or jump back and forth, $\phi(t)$ and $\theta(t)$ have to be continuous functions. Moreover, dynamic soaring should be sustainable, i.e. the average total energy should not decrease. To achieve that, the glider should choose a repetitive trajectory, which implies the control input $\phi(t)$ and $\theta(t)$ should be periodic functions. To solve the dynamic soaring problem, functions of $\phi(t)$ and $\theta(t)$ that satisfy the requirement above should be found.

Given the complexity of the model, it is not easy to find analytical functions of $\phi(t)$ and $\theta(t)$ that can achieve dynamic soaring. A control strategy can be considered to approach the problem. It is to discretize $\phi(t)$ and $\theta(t)$ into sequences corresponding to sequential small time steps. In other word, $\theta(t)$ and $\phi(t)$ are approximated by affine linear interpolation functions. It reduces the solution space by representing continuous functions with $\mathbf{countable\,many\,points}$ of control inputs. Discretization of control input function also make it more compatible with the discrete numerical model. Many previous researches [8][15][6][2][4] apply this method and solve the dynamic soaring problem by optimizing the total energy over ϕ_i and θ_i, where $i = 1, 2, 3, ..., N$ are the index for each time step in a flight period.

3.2 Optimization Setup

Section 2.4 states that dynamic soaring problem is a nonlinear system optimization problem. In this section, optimization is set up. To define the optimization variable χ, recall that the optimizer would search optimal control input $\phi(t_i)$ and $\theta(t_i)$ for each time step t_i. Then the solutions of the input $\phi(t)$ and $\theta(t)$ are piecewise affine function of time t. Since the total time for a period is unknown, the time step size Δt is also included as one of the optimization variables. They can be summarized as

$$\chi = (\phi_1, \phi_2, ..., \phi_n, \theta_1, \theta_2, ...\theta_n, \Delta t) \tag{3.1}$$

where n is the number of time steps for one period of dynamic soaring flight. There are a total $2n + 1$ optimization variables. To set up a cost function J, note that the states y, z, ψ, γ, V must be the same in their initial and final time steps to make sure the dynamic soaring is sustainable by flying in the same trajectory for the following period. Then a candidate cost function J_1 can be defined as

$$J_1(\chi) = \mathbf{s_1}^T \mathbf{W} \mathbf{s_1} \tag{3.2}$$

where,

$$\mathbf{s_1} = [y_0 - y_n, z_0 - z_n, \psi_0 - \psi_n, \gamma_0 - \gamma_n, v_0 - v_n]^T$$

and

$$\mathbf{W} = \text{diag}(W_1, W_2, W_3, W_4, W_5)$$

are weights. Notice that the energy in the beginning and the end of the period is unchanged if J_1 is optimized to its possible maximum value, which is 0. Another candidate cost function J_2 is a modified J_1 as

$$J_2(\chi) = \mathbf{s_2}^T \mathbf{W} \mathbf{s_2} \tag{3.3}$$

where,

$$\mathbf{s_2} = [y_0 - y_n, z_0 - z_n, \psi_0 - \psi_n, \gamma_0 - \gamma_n, v_n]^T$$

and

$$\mathbf{W} = \text{diag}(W_1, W_2, W_3, W_4, W_5)$$

The only difference is that the last element of $\mathbf{s}$ is changed to be v_n, which becomes a measure of kinetic energy gained. J_2 allows the final velocity to be larger then the initial velocity. J_2 encourages the optimizer to find solution that extract energy from the wind field. However, the same control policy is not sustainable, because the initial condition, the airspeed in particular, of the next period is different. Since the optimization variables are control inputs, the constraints of the optimization, in this case, are upper and lower bounds of allowable bank angle, bank rate, pitch angle, and pitch rate. Then, the optimization process for asymptotic trajectory can be formulated as,

$$
\begin{aligned}
\underset{\chi=(\phi_i,\theta_i,\Delta t)}{\text{minimize}} \quad & J(\chi) \\
\text{subject to} \quad & |\phi_i| \leq \phi_{max}, \\
& |\theta_i| \leq \theta_{max}, \\
& |\phi_i - \phi_{i+1}| < \dot{\phi}_{max}\Delta t, \\
& |\theta_i - \theta_{i+1}| < \dot{\theta}_{max}\Delta t, \\
& |\Delta t - \Delta t_0| \leq \delta_{\Delta t}, \\
& \dot{\mathbf{x}} = f(\mathbf{x}, \mathbf{u})
\end{aligned}
$$

for $i = 1, 2, ..., n$, where $J(\chi)$ can be chosen as J_1 in equation 3.2 to maintain velocity, or J_2 in equation 3.3 to extract as much energy as possible. And $f(\mathbf{x}, \mathbf{u})$ is the dynamics of the system given in chapter 2.

3.3 Simulation Results

In this section, the results of the optimization generated by Matlab's fmincon optimization toolkit is shown and discussed. The wind field parameters are set to be $\delta = 1.1$ and $w_o = 0.6$. The wind field is shown in Figure 2.4 as an example in the previous chapter. The optimization variables χ is chosen according to equation 3.1, which are all the control input ϕ and θ at each time step and the time step size. Figure 3.1 and 3.2 shows the flight trajectory and the details of states and control input applying the cost function J_1 defined in equation 3.2, which penalizes the difference between all the initial and final states except the traveling direction state x. The top left plot in Figure 3.2 shows the altitude $z(t)$ as a function of time. The bottom left plot shows the airspeed $V(t)$ as a function of time. With the vehicle starts at the nadir ($z(0) \approx -7m$) of the trajectory, it files into the wind and pulls up until it reaches the peak ($z(10.5) \approx 5m$). The airspeed decreases as the vehicle flies up to trade potential energy from kinetic energy except at the altitude $z \in (-1, 1)m$ at $t \in (3, 4)s$, where it experiences the maximum wind shear. As the vehicle crosses the wind shear, the airspeed V does not decrease much while the altitude increases at the same time, which is the key for a successful dynamic soaring cycle. After $t = 5.5s$, the vehicle turns away from the wind and descends back to its initial altitude. The airspeed at the end of the cycle reaches back to its initial value. The vehicle is able to extract energy from the wind shear. The top right plot shows the top view of the actual flight trajectory. It is clear that the vehicle is able to fly back to its initial location of the cycle. The bottom right plot shows the corresponding control input bank angle $\phi(t)$ and pitch angle $\theta(t)$ and the state of flight path angle $\gamma(t)$ as functions of time. The entire cycle takes about 10 seconds. It is in no doubt a successful dynamic soaring cycle. Altitude, airspeed, flight path angle, bank angle and y-coordinate returns to its initial value at the last time step of a cycle.

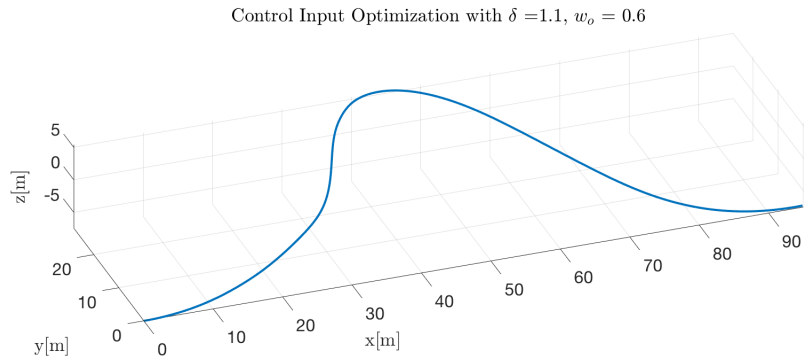

Figure 3.1: Asymptotic Trajectory with Cost J_1, $\delta = 1.1, w_o = 0.6$

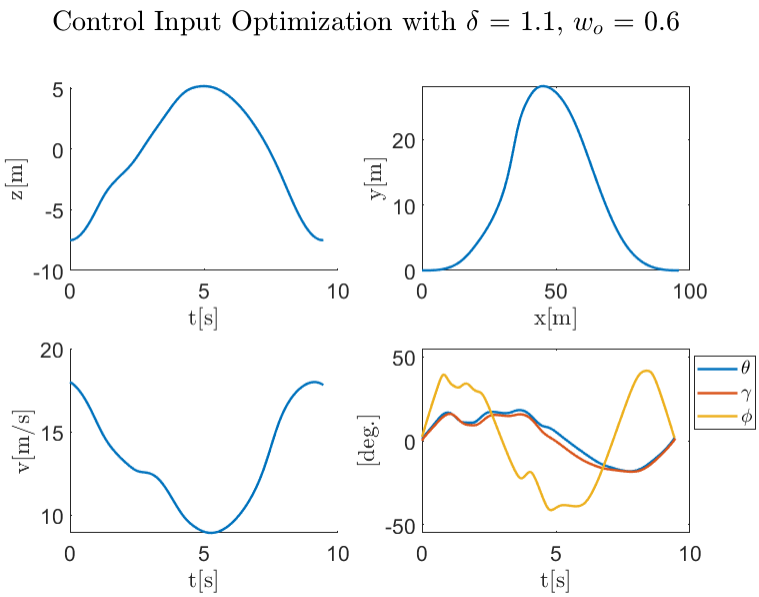

Figure 3.2: Asymptotic Trajectory Solution with Cost J_1, $\delta = 1.1, w_o = 0.6$

The simulated flight result using the cost function J_2 (equation 3.3) is shown in Figure 3.3. It is also a successful dynamic soaring cycle with substantial increase in its final airspeed from 18 m/s to 19 m/s. Also, the control input is considerably more smooth than that under J_1, with which the optimizer tries to meet the initial condition by adding unnecessary high frequency noise

to damp out extra energy the aircraft should have obtained from the wind field. Also note that the optimizer under J_2 cost tends to choose actions at the boundary of the constraint—the maximum and minimum of the bank angle, the maximum bank and pitch rate.

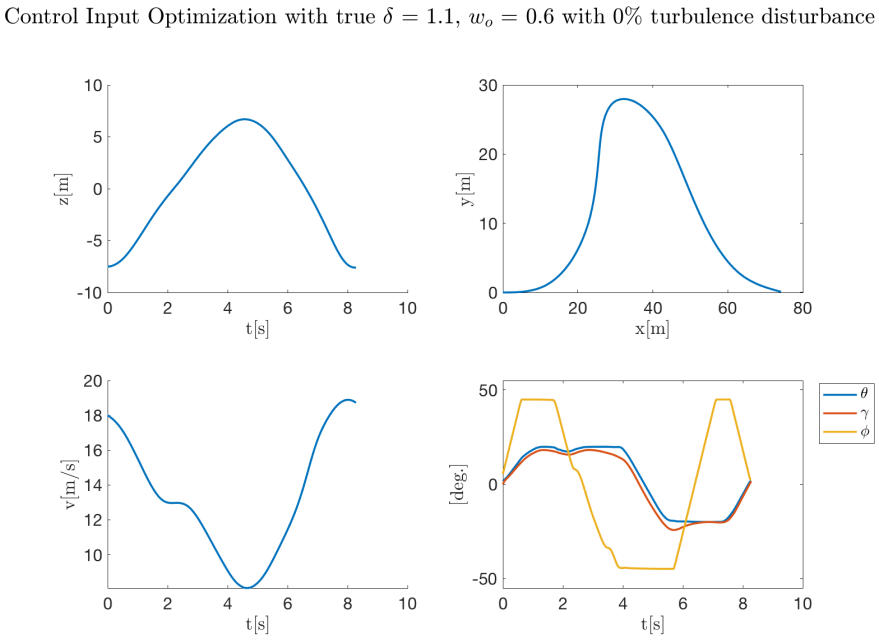

Figure 3.3: Asymptotic Trajectory Solution by Direct Optimization with Cost J_2, $\delta = 1.1, w_o = 0.6$

The corresponding optimization result for a different wind field—with $\delta = 1.0, w_o = 0.8$ is shown in Figure 3.4 and Figure 3.5 using the cost function J_1. As shown in dimensional wind profile in Figure 2.4, the overall wind speed of this wind field is larger and the shear is stronger. It infers that the aircraft is able to extract more energy from the wind field. As it is indicated in the airspeed versus time plot, at $t \in [1.9, 3.2]$ when the aircraft flies through the shear, the velocity increases while the altitude increases. With J_1 as the cost function, the optimizer amplifies noise in the control input schedule to damp out extra energy in comparison to that in Figure 3.2.

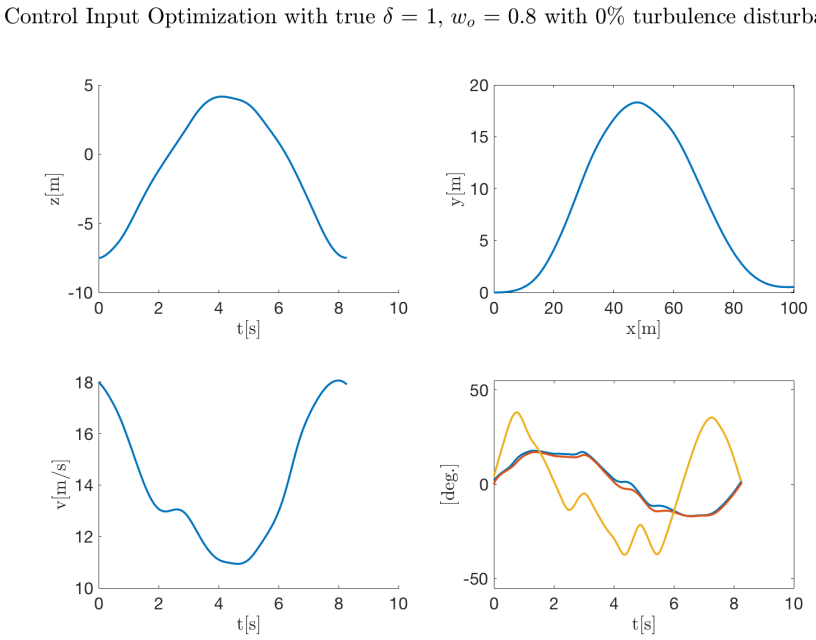

Figure 3.4: Asymptotic Trajectory Solution with Cost J_2, $\delta = 1.0, w_o = 0.8$

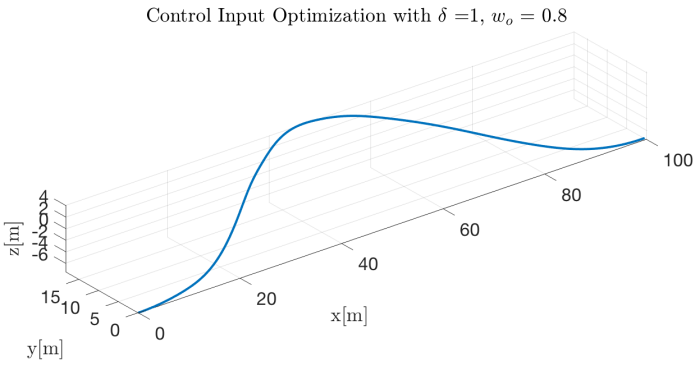

Figure 3.5: Asymptotic Trajectory Solution by Direct Optimization with Cost J_1, $\delta = 1.0, w_o = 0.8$

On the other hand, the optimization result of using the cost function J_2 is shown in Figure 3.6. With a stronger wind field, the aircraft extracts more energy from the wind field, as shown not only in a larger and longer increases of air velocity when it flies through the main shear, but also in its

final air velocity obtained. The final airspeed increases to about $20m/s$ in comparison to $19m/s$ shown in Figure 3.2.

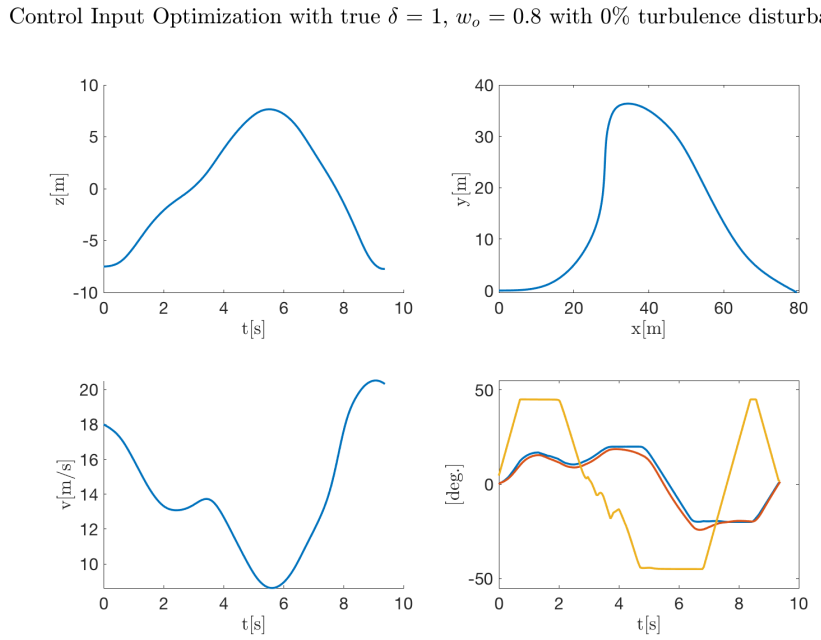

Figure 3.6: Asymptotic Trajectory Solution n with Cost J_2, $\delta = 1.0, w_o = 0.8$

Although this thesis only shows the simulation in two selective wind field, the optimization can also find a solution in other wind field with sufficiently strong shear and proper initial values chosen.

Chapter 4

Conclusion

This thesis verifies an optimization process to find a solution of asymptotic dynamic soaring in a fixed wind shear. A numerical simulation is built and the optimization process is discussed in details. The simulated result shown in the last chapter shows that the optimization process can indeed generate a control input schedule to achieve asymptotic dynamic soaring. In the simulation, the aircraft can maintain flight without thrust.

Although this optimization process can successfully find dynamic soaring, it is not as ideal in practice as it is theoretically. The first limitation is the size of optimization variables, which grows linearly with the number of the interpolation points ϕ_i and θ_i. Thus, there is always a trade-off between the solution space expression capability and the complexity of the optimization. In practice, the computation complexity makes it impossible to generate a solution on the fly. Secondly, there is no guarantee that the nonlinear optimizer can find the global maximum. Thirdly, in this thesis the wind field is assumed fixed and time-invariant. In reality, however, wind field is stochastic due to turbulence and other unmodeled factors in the environment. Since the solution as control input schedule is open-looped, disturbance from the wind field can leads to failure in dynamic soaring. These are the issues needed to be addressed to make autonomous dynamic soaring possible in reality. For the first issue, the imminent 5G communication technique with fast and little time delay network might be helpful by conducting the optimization computing in the cloud instead of the onboard computer. At the same time, some modern algorithm, like those in the field of artificial intelligence, might resolve the last two issues.

Bibliography

[1] J. Bird, J. W. Langelaan, C. Montella, and J. Spletzer, "Closing the loop in dynamic soaring," *AIAA Guidance, Navigation, and Control Conference*, 2014.

[2] G. Sachs and B. Gruter, "Dynamic soaring at 600 mph," *AIAA Scitech Forum*, 2019.

[3] J. Bird, "Wind estimation and closed-loop control of a soaring vehicle," *M.S. Thesis, Penn State University*, pp. pp.46–48, 2013.

[4] N. Long and S. Watkins, "Regenerative dynamic soaring trajectory augmentation over flat terrains," *AIAA Scitech Forum*, 2019.

[5] L. Rayleigh, "The soaring of birds," *Nature*, vol. 27(701), pp. pp. 534–535, 1883.

[6] G. Sachs and B. Gruter, "Maximum travel speed performance of albatrosses and uavs using dynamic soaring," *AIAA Scitech Forum*, 2019.

[7] P. Jouventin and H. Weimerskirch, "Satellite tracking of wandering albatrosses," *Nature*, vol. 343, pp. pp.746–748, 1990.

[8] P. Jouventin and H. Weimerskirch, "Sustained fast travel by a grey-headed albatross (thalassarchie chrysostoma) riding an antarctic storm," *The Auk*, vol. 121, pp. pp.1208–1213, 1990.

[9] M. Deittert, A. Richards, C. A. Toomer, and A. Pipe, "Engineless unmanned aerial vehicle propulsion by dynamic soaring," *AIAA Journal of Guidance, Control, AND Dynamics*, vol. 32, 2009.

[10] G. Bousquet, "Dynamic soaring in finite-thickness wind shears: an asymptotic solution," *AIAA Guidance, Navigation, and Control Conference*, 2017.

[11] N. Garvilovic, "Bioinspired energy harvesting from atmospheric phenomena for small unmmaned aerial vehicles," *AIAA Scitech Forum*, 2019.

[12] M. C. and S. J., "Reinforcement learning for autonomous dynamic soaring in shear winds," *RSJ International Conference on Intelligent Robots and Systems*, pp. pp. 534–535, 2014.

[13] F. Hendricks, "Dynamic soaring," *Ph.D Thesis, University of California, Los Angeles*, 1972.

[14] M. Boslough, "Autonomous dynamic soaring platform for distributed mobile sensor arrays," *Sandia National Laboratories*, 2002.

[15] G. Sachs, "Minimum shear wind strength required for dynamic soaring of albatrosses," *IBIS*, pp. pp. 1–10, 2005.

Zhenda Li

Education

Schreyer Honor College, The Pennsylvania State University, University Park, PA, USA
M.S. in Aerospace Engineering *(Anticipated Graduation: Dec. 2019)*
B.S. in Aerospace Engineering & Minors in Electrical Engineering & Computational Science *(May 2018)*

Work & Research Experience

Researcher || Reinforcement Learning Algorithm Design *(2018 ~ current)*

- Developing reinforcement Learning Algorithm for high dimension continuous action space
- Apply reinforcement learning algorithm in structural diagnostic and UAV trajectory planning problems

Researcher || Unmanned Air Vehicle (UAV) Dynamic Soaring *(2017 ~ current)*

- Developed computer programs to simulate flight dynamics for a fixed-wing glider UAV under wind shear
- Optimized flight trajectory to achieve dynamic soaring (DS)--fly technique, inspired by albatross' soaring, to gain kinetic energy by repeatedly crossing wind shear
- Authoring a graduate thesis, in which control law is proposed and implemented to achieve DS
- Applying reinforcement learning algorithm to find best trajectory

Simulation Assistant || Penn State Computational Reacting Flows Lab *(Summer 2017)*

- Designed and run numerical simulation experiments (LES and DNS) in turbulent combustion flame using high-performance computing (HPC) and visualized the computing results
- Interpreted computational result to help understanding the physics of interaction among small-scale vortices, flamelet, and chemical species and compared it to the theoretical prediction in state of art

Software Engineer (Intern) || Heshun Hardware Ltd. in Guangdong, China *(Summer 2016 & Summer 2018)*

- Programed software to model and calculate stress, strain, and safety factor of warehouse rack components to help select the structurally stable type of production with the least cost and meet the national safety standard. Delivered the software to the employer and shortened hours in per decision time
- Trained and tested an automatic 6 DOF welding robot to complete welding tasks on several complex parts. Communicated and instructed corresponding technicians in robotics' functioning and maintenance

Teaching Assistant || for ARESP424 Advanced Computer Programming *(2019 ~ current)*

Design & Manufacture Experience

Competitor || American Helicopter Society (AHS) Student Design Competition *(2017 ~ 2018)*

- Won the 3rd place in the undergraduate section worldwide by designing wing, airfoil, and aerodynamic control surfaces for a reconfiguration UAV aircraft to reduce aerodynamic drag predicted using XFlr5
- Performed stability analysis, optimized trajectory, designed control law, and simulated flight dynamics

Team member || Sailplane Group in Penn State *(2016 ~ 2018)*

- Designed and upgraded wing sections of a human power aircraft (HPA) aiming to Kremer Prize
- Led and guided other members to build, test, repair, and realize the designed wing sections
- Cooperated with other members to construct carbon fiber keel and the main boom of the HPA

Member || Formula SAE in Penn State *(2015 ~ 2016)*

- Built CAD models using SolidWorks and fabricated parts for a race car in lathe and other machining
- Fabricated mould of race car shell, diffuser, and spoiler with foam and glass fiber

Skills, Programming Languages & Coursework

- Python, C++, Matlab, Linux, Pytorch, Tensorflow, Mathematica
- Fluid Mechanics, Dynamics, Control Theory, Machine Learning, Reinforcement Learning, Numerical Methods, Aerial Vehicle Design, Robotics, State Estimation & Kalman filter
- Chinese and Cantonese speaking, reading, and writing